Automated Iterative Three-Dimensional Registration of Positron Emission Tomography Images

Carl K. Hoh, Magnus Dahlbom, Greg Harris, Yong Choi, Randall A. Hawkins, Michael E. Phelps and Jamshid Maddahi

Division of Nuclear Medicine and Biophysics, Department of Molecular and Medical Pharmacology, Department of Radiological Sciences, Laboratory of Nuclear Medicine (DOE)*, The Crump Institute for Biological Imaging, School of Medicine, University of California, Los Angeles, California

Two types of image similarity measures, the sum of absolute differences (SAD) and the stochastic sign change (SSC), were compared for three-dimensional registration of images from PET. To test the accuracy of both registration methods, 30 FDG brain studies, 40 ^{13}N-ammonia cardiac studies and 20 FDG liver tumor studies (where each image set contained 15 image planes, 128 × 128 pixels per plane) were made into worse case conditions by creating image sets of low counts and extreme defects. These images were then registered to the reference images that had been moved in three dimensions into a random set of known translations, rotations and normalization factors (x, y, z, θ, ρ, σ, nf). Neither method required any external fiduciary markers or operator interventions to register a set of images. The optimization of the image similarity (using the SAD or SSC) was performed with the simplex method and registration was completed within 10 min of computation time on a low-end workstation. Overall, the SAD method had an average inplane (x, y) registration error of 0.5 ± 0.5 mm, a z-axis registration error of 1.1 ± 1.1 mm, an inplane rotational error of 0.5 ± 0.4 degrees, an out-of-plane rotational error of 1.1 ± 1.2 degrees and a normalization factor error of 0.015 ± 0.016. The SSC method had an average inplane (x, y) registration error of 0.6 ± 0.5 mm, a z-axis registration error of 1.1 ± 1.1 mm, an inplane rotational error of 0.7 ± 0.5 degrees, an out-of-plane rotational error of 1.0 ± 1.2 degrees and a normalization factor error of 0.014 ± 0.014. This study demonstrates that either the SAD or SSC method for measuring image similarity, combined with the simplex method for function optimization, are accurate methods for registration of a wide variety of PET images including low count studies and those with marked interval changes in the pattern of count distribution.

J Nucl Med 1993; 34:2009-2018

In comparing serial PET images, as with serial medical images in general, image registration is often performed visually. In most cases, this visual registration is facilitated by using known structural landmarks or object contours as anatomical references. In quantitating serial PET studies, accurate image registration is important to allow application of a common region of interest (ROI). Significant errors in the estimates of the glucose metabolic rate by ROI analysis have been shown to occur with only a 1-pixel (2.8 mm) shift in ROI placement (1). The capability to register PET images is also important for correcting patient movement in between serial emission studies so that a single transmission scan can be applied in the reconstruction of both emission scans. It has been recently reported, that even 0.5-cm misalignments between the transmission image and the emission image can cause significant changes in the apparent distribution of radiotracer activity in the myocardium (2,3).

Various methods of iterative image registration have been described (4–8). In most algorithms, one image is kept stationary as a reference image while the image to be registered is resampled (resliced) into a new spatial orientation determined by a set of registration parameters: three translational (x, y, z) and three rotational (inplane: θ; coronal: ρ; and sagittal: σ) movements. The basic components of image registration consist of: (1) resampling one of the image sets using a set of registration parameters; (2) measuring of the amount of similarity between the resampled image and the reference image; and (3) finding the optimum set of registration parameters by maximizing the similarity measure between the two images.

The sum of absolute difference (SAD) is a simple image similarity measure, where after subtraction of the two image sets, the absolute difference of all the pixels in the subtraction image is summed (4). Lower SAD values represent more similar image sets, and a zero SAD represents exactly similar images.

Another, perhaps more robust method for measuring image similarity is the stochastic sign change (SSC), originally described by Venot (6). This similarity measure has

been applied to the normalization and registration of digital subtraction angiograms (9), planar scintigraphic images (10,11) and the registration of two-dimensional electron micrographs (12). Recently, this method has been described for the correction of translational and inplane and coronal rotational misalignments of PET brain images (13). However, this implementation of the SSC measure did not account for rotational misalignments in the sagittal (σ) plane.

To apply the SSC method, at least one of the images is required to contain a significant amount of poisson distributed noise, or that a small (5%) periodic change in grey scale intensities is added to each pixel along each horizontal row of one of the image sets, similar to the deterministic sign change (DSC) described by Venot (14). After subtraction of the two image sets, the SSC is determined by searching along each pixel row and counting the number of times the pixel grey scale goes from negative to positive or from positive to negative. At optimum registration there is a maximum total sign change (14).

In this study, we implemented and compared the accuracy of the SAD and SSC methods as image similarity measures to account for all possible movements in three dimensions (x, y, z, θ, ρ, σ), as well as the normalization factor (nf).

MATERIALS AND METHODS

Experimental Design

The overall experimental design was to evaluate the two registration algorithms applied to brain, cardiac and liver PET images. Two separate but consecutive acquisitions were utilized, which were then misaligned with known parameters in three-dimensional space.

In order to test the robustness of the algorithms, low-count images were used for registration. In addition, in a subset of experiments, large defects were simulated in one of the image sets in order to create dissimilarities between the images before registration. In order to assess the effects of smoothing, registration of brain studies were done with and without nine-point smoothed images.

PET Images

All isotopes (FDG and ¹³N-ammonia) were produced at the biomedical cyclotron facility at UCLA. The labeling of 2-deoxyglucose with ¹⁸F (substitution of hydrogen with ¹⁸F in the 2 position) provided the positron emitting form of the glucose analog.

All PET images were randomly selected among clinical studies which were acquired on a Siemens/CTI 931/08-12 whole-body PET system (CTI, Inc., Knoxville, TN). This is an eight-ring system, which simultaneously acquires 15 transaxial image planes (128 × 128 pixels per plane; 6.75-mm plane separation).

Brain Studies

The brain studies were performed with 10 mCi of FDG. Attenuation correction was provided by a threshold detection algorithm (15), eliminating the need for transmission imaging of the brain images. Following a 40-min uptake period after intravenous administration of FDG, emission images were acquired in eight 5-min frames.
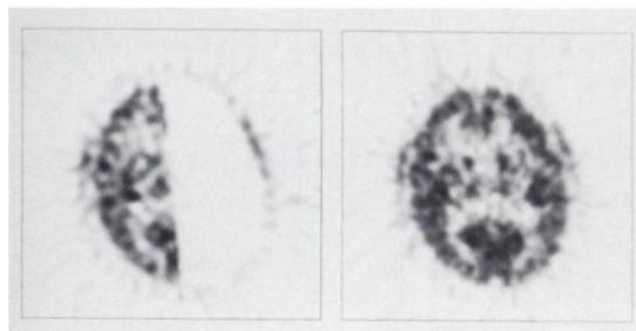

FIGURE 1. Examples of FDG-PET brain image sets extracted from a dynamic acquisition. Each image set contains a total of 15 image planes. Only one representative image plane (plane 7) is shown from the simulated hemispherectomy image set (left image) and from the reference image set (right image). Since each frame was 5 min in duration, there was less than 1.5 million total counts in each extracted image. Since no visible movement occurred between the two image frames, quantification of the registration error was possible when known three-dimensional movements were applied to the reference image set.

Registration of Ten Low-Count PET-FDG Brain Image Sets. The low-count PET brain images were created by extracting two 5-min frame acquisitions from a patient study where no visually detectable movements occurred between the two adjacent frames. This extracted brain image set (15 planes) had approximately 6.7 million total counts. These images were reconstructed with a 0.30 cycles/pixel Shepp-Logan filter, and zoomed to 2.55 giving a transaxial pixel width of 1.84 mm. One of the image frames was resampled into ten random but known sets of misalignments, and then the other image frame was registered onto these misaligned images.

Registration of Ten Low-Count PET-FDG Brain Images with Preregistration Smoothing. To test the effect of image smoothing prior to registration, the low-count brain images in one set were nine-point smoothed with a (3 × 3) filter kernel that contained all ones. The reference brain images were not smoothed with this filter since they were already smoothed by the misalignment resampling program. The smoothed images were then registered onto these misaligned images.

Registration of Ten Low-Count FDG-PET Brain Image Sets Where One Set Contained a Simulated Hemispherectomy and a Different Reconstruction Filter. To test the effect of a severe brain defect and a dissimilar reconstruction filter on the accuracy of registration, a single 5-min brain image was reconstructed to a 128 × 128 by 15-plane image matrix with a ramp 0.30 cycle/pixel filter and zoom of 2.55. The corresponding reference image frame was reconstructed with a 0.30 cycle/pixel Shepp-Logan filter and resampled into ten known but random misalignments. In the image set with the ramp filter, a hemispherectomy was simulated by using the interactive drawing/painting program which allowed an operator-drawn region that encompassed the entire left hemisphere to decrease pixel grey scale values to zero (Fig. 1). This process was applied to all image planes containing the left cerebral hemisphere. These "hemispherectomy" images were then registered to the resampled reference image set.

Cardiac Studies

Rest and stress ammonia myocardial perfusion studies were performed with 20 mCi of sterile ¹³N-ammonia. Attenuation correction was accomplished with a 20-min transmission scan. Each

image was acquired for 20 min, beginning 7 min after injection of ammonia. Pharmacologic stress was induced by constant infusion of adenosine (at a rate of 140 μg/kg/min) for 6 min and ^{13}N-ammonia was injected 3 min into adenosine infusion.

Cardiac images were reconstructed into a 128 × 128 by 15-plane image matrix using a 0.15 cycle/sec Shepp-Logan filter and were zoomed to 3.0 giving a transaxial pixel width of 1.56 mm.

To account for any movement between the rest and stress images, we recorded the baseline misregistration between the two image sets as measured by the SAD and SSC technique, and assumed that any additional misalignments that were induced with the resampling program would be a linear addition to the baseline misregistrations.

Registration of Ten Rest and Stress Nitrogen-13-Ammonia Cardiac PET Image Sets. The rest image was moved with respect to the stress image by resampling it in ten different random but known sets of misalignments. The stress image was registered onto the ten misaligned rest images.

Registration of Thirty Nitrogen-13-Ammonia Cardiac PET Image Sets Where the Stress Images Contained Large Simulated (Anterior, n = 10; Lateral, n = 10; and Inferior, n = 10) Perfusion Defects. Simulated stress perfusion defects were created on the adenosine stress images of one set using an interactive drawing/painting program which allowed operator-drawn regions to decrease enclosed pixel grey scale values by 50%. These regions were drawn on all image planes containing anterior, lateral or inferior myocardial activity of the stress studies so that three abnormal studies were generated: one study with a large anterior wall perfusion defect, one with a large inferior wall perfusion defect and another with a large lateral wall perfusion defect (Fig. 2). These simulated defect images were then registered to the resting image sets which had been resampled into 10 random sets of misalignments.
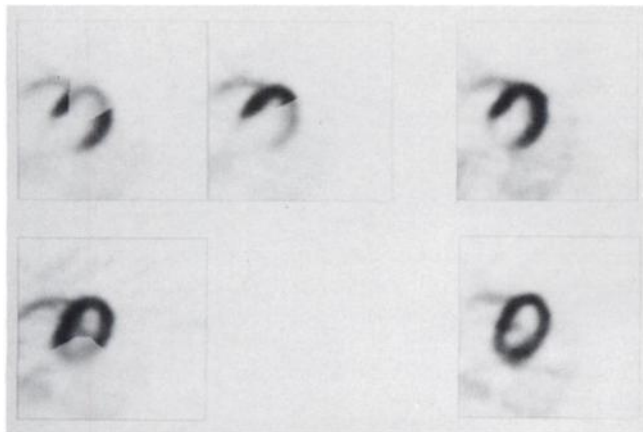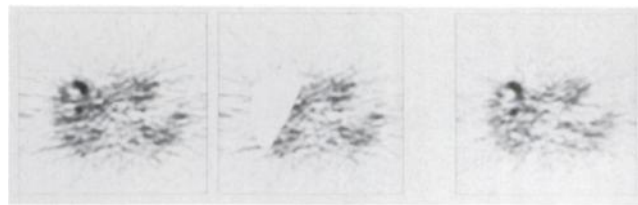

FIGURE 3. Examples of low count FDG liver tumor image sets extracted from a dynamic FDG-PET liver acquisition. A 15-plane image set, of 4-min duration, was created by extracting one image frame from a dynamic acquisition. This image contained less than 1 million total counts. One representative image plane is shown from the image set of a metastatic tumor (left image) and from the image set containing a simulated resection (middle image). The reference image (right image) was extracted from another image frame of the dynamic acquisition. No visible movement occurred between the two image frames, so that known three-dimensional movements applied to frame 30 permitted the quantification of the error when registering frame 29 to frame 30.

Liver Studies

The liver studies were performed with 10 mCi of FDG. Attenuation correction was accomplished with a 20-min transmission scan. The last two 4-min frames from a 60-min dynamic FDG study of a patient with metastatic melanoma of the liver were extracted to create two low-count FDG liver images (approximately 4.5 million counts in each image set). The liver images were reconstructed to a 128 × 128 by a 15-plane image matrix using a 0.30 cycle/sec Shepp-Logan filter and were zoomed to 1.5, giving a transaxial pixel width of 3.13 mm.

Registration of Ten FDG-PET Liver Image Sets. The last frame of the liver study was assigned as the reference image and was resampled into ten random but known sets of misalignments. The second-to-last frame was then registered onto the ten misaligned reference images.

Registration of Ten FDG-PET Liver Image Sets Where One of the Image Sets Had Both the Tumor Lesions and a Portion of the Liver Removed. Large liver defects (>20% of liver volume) were simulated in the last image frame using the interactive drawing/painting program, such that both tumor and a large portion of liver pixels were set to zero (Fig. 3). This image was then registered to the reference liver image which was resampled into ten random sets of parameters using the resampling program.

Theoretical Methods

Creation of Misaligned Images with Known Misregistration Parameters. To test the accuracy of the SAD and SSC registration algorithms, known misalignments between two similar image sets were needed, so that the misregistration values detected by the automated registration programs could be compared to the known actual values. For FDG-PET brain and liver images, this was accomplished by extracting two image frames from a dynamic study and confirming there was no visible evidence of movement after subtraction of the two image frames. For the rest and adenosine stress ^{13}N-ammonia cardiac studies, it was expected that small misalignments probably had occurred due to the length of the cardiac PET acquisition protocol which typically spanned over 2 hr even though no misregistration was visible after subtraction. These subpixel "baseline" misalignments were also taken into account in the analysis of the results of simulated movements. Since normal cardiac studies were selected, it was assumed that there was no change in cardiac size.

FIGURE 2. Examples of ^{13}N-ammonia cardiac image sets used for simulating the registration of cardiac images with severe perfusion defects. The perfusion defects were created with a user-generated ROI program on several image planes of each stress image set which contains a total of 15 image planes. One representative image plane is shown for a simulated anterior perfusion defect (left upper image), simulated lateral perfusion defect (upper middle image) and a simulated inferior perfusion defect (lower left image). Plane 9 (upper right image) and plane 10 (lower right image) from the resting study show the corresponding reference images used for registration.

image to register — **reslice** → (x_i, y_i, z_i, θ_i, ρ_i, σ_i, nf_i) → **resliced image**   **reference image**

→ **subtraction**

subtraction image → **SAD** $_i$

(x_{i+1}, y_{i+1}, z_{i+1}, θ_{i+1}, ρ_{i+1}, σ_{i+1}, nf_{i+1})

simplex method of optimization

$$SAD_1 = f (x_1, y_1, z_1, \theta_1, \rho_1, \sigma_1, nf_1)$$
$$SAD_2 = f (x_2, y_2, z_2, \theta_2, \rho_2, \sigma_2, nf_2)$$

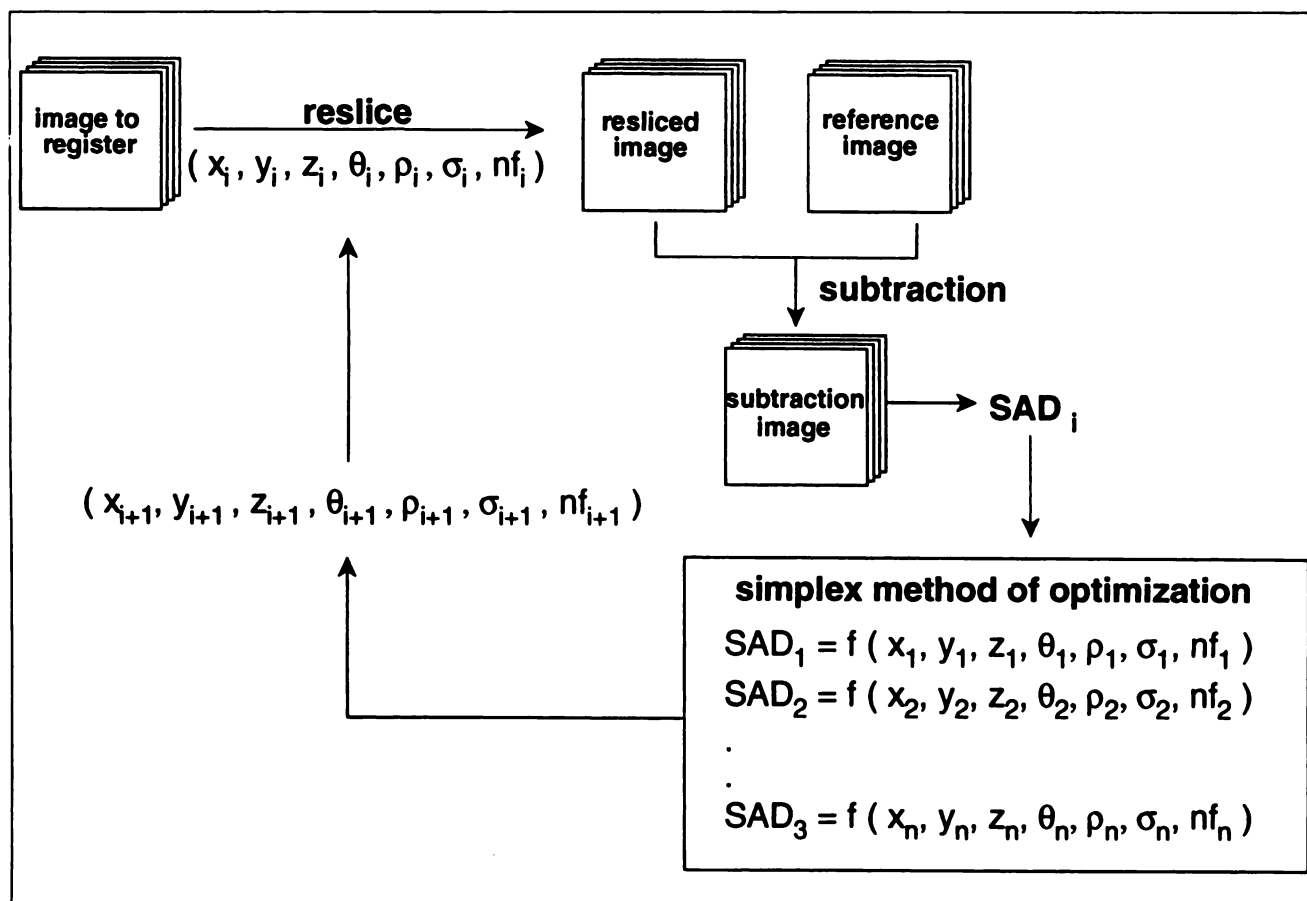$$SAD_3 = f (x_n, y_n, z_n, \theta_n, \rho_n, \sigma_n, nf_n)$$

FIGURE 4. Diagram of the processing algorithm for iterative registration using the SAD method of image similarity. For the SSC method, a similar diagram can be made where the SSC method replaces the SAD method for image similarity measure. In both methods, the image to be registered was resliced by a set of parameters (x, y, z, θ, ρ, σ and nf) so that it could be compared to the reference image set. After a pixel by pixel subtraction and determination of the similarity measure of each corresponding image plane, a total similarity measure is generated by summing of the similarity measures from each plane. Each set of reslice parameters (x, y, z, θ, ρ, σ and nf) gave a SAD or SSC value, which allowed the simplex method to determine a new set of estimated parameters for reslicing.

By using a resampling program, the reference image (Fig. 4) was created by trilinearly interpolating each pixel in an entire 15-plane image dataset to a known set of misaligned reference parameters (x, y, z, θ, ρ, σ, nf). The resampling program allowed all parameters to be simultaneously and randomly altered so that complex three-dimensional movements could be accurately simulated. The random generation of misalignment values ranged from ±8 pixels (±25 mm to ±12 mm depending on the image zoom) in the x and y directions; ±6.75 mm in the z direction; ±12 degrees in the θ, ρ and σ rotational directions; and from 0.82 to 1.34 normalization factors. In the registration algorithm, these misaligned reference images were kept stationary while the second image, the "image to register" in Figure 4, was iteratively resampled (with trilinear interpolation) to a new set of estimated registration parameters (x, y, z, θ, ρ, σ, nf) until there was a convergence to a minimum SAD or maximum SCC value. The errors in the automated registration programs were defined as the absolute differences between the known and detected misregistration parameters.

Iterative Optimization Algorithm. Since the SSC is a stochastic function of the registration parameters, it is a nonlinear and non-differentiable function. This makes the maximization of the SSC more difficult than discrete parametric measures of image similarity, such as the SAD, the correlation coefficient or the correlation

function (*14*). The nondifferentiable characteristics of the SSC function prevented the implementation of rapid gradient type search algorithms to maximize the SSC and special optimization algorithms were required (*14*).

Although the SAD similarity measure is known to be not as accurate as the SSC similarity measure (*16*), we expected the SAD method to converge to a set of registration parameters (x, y, z, θ, ρ, σ, nf) such that it was possible to then switch to the SSC method for further convergence to the true registration values. This would avoid a global parameter space optimization using the SSC similarity which could converge onto a local rather than a global SSC maximum. At the same time, we could compare the differences in the registration errors of the two methods.

The overall registration algorithm is shown in Figure 5. For a given set of registration parameters (x, y, z, θ, ρ, σ, nf) a function value (SAD or SSC value) was calculated. By initially creating a collection of 17 sets of random registration parameters with their 17 corresponding similarity function values (SAD or SSC), a "cloud" of points in seven-dimensional space was formed, from which the simplex method for function optimization could be used (*17*). The simplex method was selected for both the SAD and SSC methods since this optimization method was easy to implement, (only one function evaluation was required for each algorithm iteration). For the SAD method, the best registration parameters
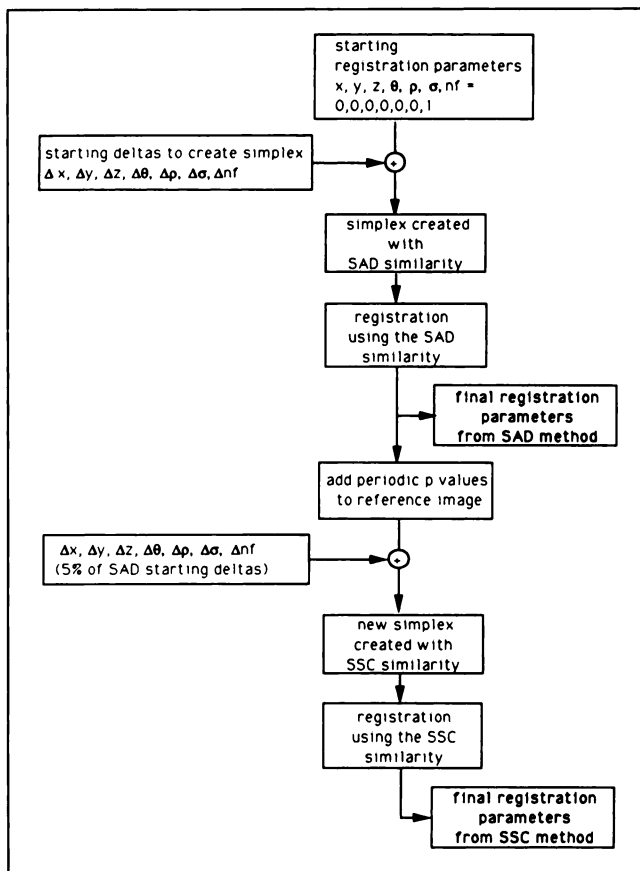
FIGURE 5. Diagram showing the overall registration algorithm to test the SAD and SSC methods of registration. A collection of 17 sets of random registration parameters and their 17 corresponding SAD similarity function values were formed by adding and subtracting various combinations of Δx, Δy, Δz, Δθ, Δρ, Δσ and Δnf to a central starting parameter. The simplex method minimized the SAD similarity measure to find the optimum parameters for registration. The images were preprocessed by adding a periodic p value (adding to each original pixel grey scale value, a row alternating positive or negative value which was 5% of the original pixel value). A new simplex was formed around the final parameter obtained from the SAD method by using Δx, Δy, Δz, Δθ, Δρ, Δσ and Δnf which were 5% of the values used in the SAD method. The simplex method then maximized the SSC similarity measure to find any improvement in the optimum registration parameters over the SAD method.

were optimized based on the minimization of the SAD similarity measure, whereas the similarity measure was maximized for the SSC method. In the SSC method, the images were preprocessed by adding a periodic p value (adding to each original pixel grey scale value, a row alternating positive or negative value which was 5% of the original pixel value). The addition of this periodic value provided sign changes required for registration (13). Although the SSC method we implemented was more similar to the deterministic sign change (DSC) described by Venot (14), we will refer to the method as the SSC.

Implementation of the Overall Registration Algorithm. The registration program was written in the C language and compiled using the standard C compiler provided on a SPARC IPC workstation (Sun Microsystems, Inc., Mountain View, CA).

The most computationally consuming steps in the registration algorithm were in the resampling of the three-dimensional volume of pixel data and the pixel by pixel determination of the similarity

measure over all image planes. To improve the speed of each iteration, selected image pixels were omitted from both the image reslicing and image similarity calculations, by using a binary image mask which had the same image matrix size and plane numbers as the reference PET image. Each pixel in this volumetric image mask referred to corresponding image pixel in the reference image. Each mask pixel contained either a value of 0 or 1, where the value of 0 flagged an omitted pixel, and the value 1 flagged a pixel to be included in the reslicing and similarity calculations. For a mask pixel to be 1, the grey scale intensity value of this pixel location in the reference image (Fig. 4) had to be above a predetermined background threshold level. A mask pixel had its value set to 0 if that same pixel location in the reference image was below the threshold. The threshold was visually selected at a level which defined the target organs/objects above background. This threshold was found to be about 15% of the maximum image pixel value for the brain studies, 20% for the cardiac studies and 10% for the tumor liver studies. From this volumetric image mask, a minimum and maximum starting and ending pixel row and pixel column was determined for each image plane further reducing the number of pixels involved with reslicing and similarity calculations.

To further improve the speed of the registration algorithm, pixel rows were skipped in both the reslicing and similarity calculations defined by Equation 1:

$$ystep = integer \ (3 \times (ymax - ymin)/64), \qquad Eq. \ 1$$

where ystep was the number of consecutive pixel rows skipped (i.e., not involved in the registration), ymax was the maximum row number and ymin was the minimum row number with a nonzero flag in the image mask. After an initial parameter and similarity measure convergence, the registration was restarted with only half of the rows skipped to improve the y direction "resolution" of the registration. At the end of each convergence, the number of skipped rows was reduced by one-half until all rows were included to "fine tune" the registration.

RESULTS

All results are described in mean and ±1 s.d.

Registration of Brain Images

Using the nine-point smoothed brain images in both the SAD and the SSC registration methods, there was improved registration shown as a decrease in the interplane translational error (z), and inplane rotational error (θ), (p < 0.05, Table 1). With the nine-point smoothed images, there was no significant difference in the registration errors between the SAD and SSC methods (Fig. 6).

The registration of ten simulated hemispherectomy brain images to a normal brain study are shown in Table 2. No significant differences in the registration errors in x, y, z, θ, ρ, σ and nf were found between the SAD and SSC methods (p > 0.05). In two simulations, the error of rotational misregistration was larger than 5 degrees and visual assessment of the subtraction images showed that the registration failed. Restarting these two cases with different initial parameters registered the images to maximum errors of: x = 1.5 mm, y = 1.5 mm, z = 4.2 mm and rotational = 2.0 degrees.
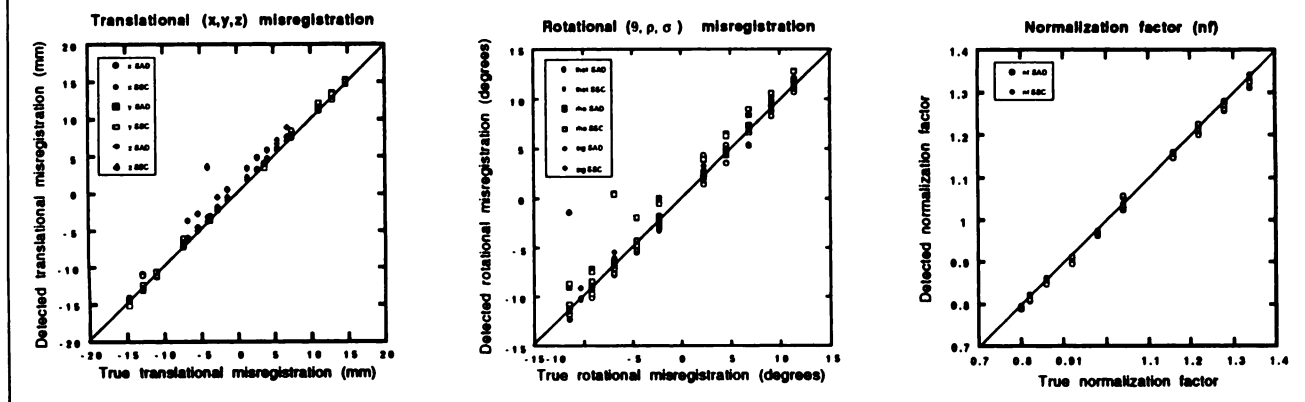
FIGURE 6. Results of detected versus true misregistration values in FDG-PET brain images where 10 image sets were smoothed with a nine-point smoothing filter, 10 image sets were nonsmoothed and 10 image sets where one set contained a simulated hemispherectomy. The diagonal line in all three graphs is the line of identity.

Registration of Cardiac Images

The results of the registration of ten normal rest/stress ^{13}N-ammonia cardiac perfusion images are shown in Table 3. The true normalization factors are not shown between the rest and stress studies because different radiotracer doses were injected for the rest and stress images, and the exact physiologic augmentation of myocardial perfusion in the adenosine stress image was not known. No significant differences in the registration errors in x, y, z, θ, ρ, σ and nf were found between the SAD and SSC methods on normal cardiac studies (p > 0.05) (Fig. 7).

The comparison of the registration errors using the SAD and SSC methods for registering the 30 cardiac studies with simulated perfusion defects is shown in Table 4. The re-

sults show that there was no significant difference in registration errors of one method over the other (p > 0.05).

Registration of FDG Liver Images

The registration errors of ten low-count FDG liver images are shown in Table 5. There was less registration error in the x direction using the SAD method than the SSC method (p < 0.001). In the other parameters, there was no significant difference between the errors in registration (Fig. 8).

The registration errors of liver images where one of the image sets contained large simulated defects is shown in Table 6. There was no significant difference in the errors of
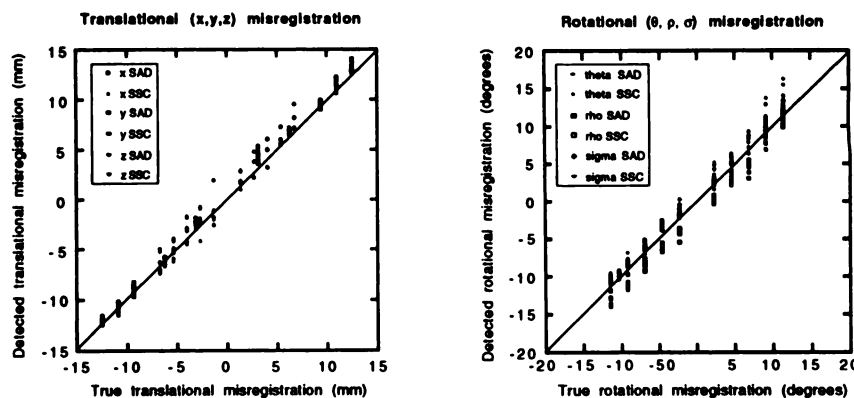

FIGURE 7. Results of detected versus true misregistration values in 40 ^{13}N-ammonia cardiac images where 10 image sets contain no perfusion defects, 10 image sets contain anterior perfusion defects, 10 image sets contain posterior perfusion defects and 10 image sets contain inferior perfusion defects. The diagonal line in both graphs is the line of identity.
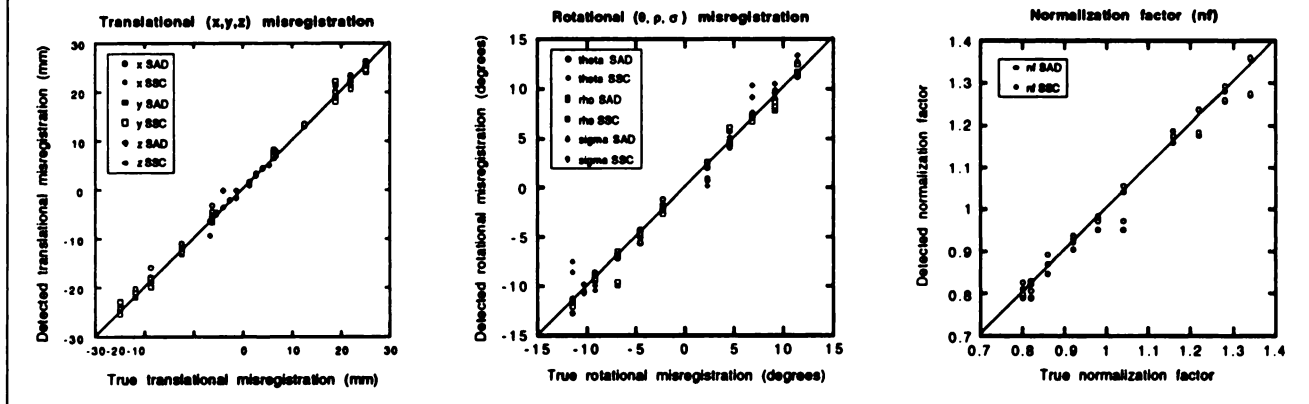
FIGURE 8. Results of detected versus true misregistration values in 20 low-count FDG liver images, where 10 of the image sets contained simulated liver defects. The diagonal line in all three graphs is the line of identity.

all parameters (x, y, z, θ, ρ, σ, and nf) between the SAD and SSC methods.

DISCUSSION

Comparison of SAD and SSC Similarity Measures for Three-Dimensional Image Registration

Although the SSC similarity measure is reported to be more accurate than the SAD method for registration, we have found that both methods were comparable in terms of registration accuracy. Moreover, both methods gave average errors of misregistration that were clinically acceptable, typically 0.5 ± 0.5 mm in the inplane direction, 1.1 ± 1.1 mm in the interplane direction and 0.9 ± 1.1 degrees for all rotational directions. The maximum registration error occurred in two hemispherectomy brain images where the

error of rotational registration was larger than 5 degrees. The final subtraction images allowed a final visual check on the registration. The occurrence of misregistration was not due to a failure in the property of the similarity measures but in the simplex optimization algorithm which converged on a local maximum rather than on a global maximum of the similarity measure. By making a small change (2%) in the threshold for creating the binary image mask, correct convergence was achieved due to the slightly different initial parameter created by the mask.

The process of registering only pixels above a selected grey scale threshold was similar to contouring (segmentation). In the Chen-Pellazari method, all object pixels (above a threshold i.e., within the contours) are conceptually reassigned a common pixel value, regardless of the

TABLE 1
Average and Maximum Errors in Registration of Low Count FDG Brain Images and Effect of a Nine-Point Smoothing Filter

	Average error ± s.d.			Maximum error	
	Nonsmoothed	Smoothed	p < 0.05	Nonsmoothed	Smoothed
x SAD (mm)	0.11 ± 0.08	0.14 ± 0.08		0.22	0.24
y SAD (mm)	0.23 ± 0.13	0.22 ± 0.12		0.41	0.39
z SAD (mm)	0.86 ± 0.13	0.44 ± 0.07	*	0.98	0.54
θ SAD (deg)	0.85 ± 0.09	0.12 ± 0.05	*	1.01	0.17
ρ SAD (deg)	0.18 ± 0.14	0.12 ± 0.07		0.40	0.20
σ SAD (deg)	0.24 ± 0.13	0.10 ± 0.08		0.43	0.26
nf SAD	0.02 ± 0.01	0.01 ± 0.00		0.02	0.01
x SSC (mm)	0.31 ± 0.21	0.24 ± 0.13		0.53	0.32
y SSC (mm)	0.20 ± 0.13	0.28 ± 0.15		0.47	0.60
z SSC (mm)	0.88 ± 0.10	0.41 ± 0.07	*	1.00	0.51
θ SSC (deg)	0.77 ± 0.23	0.25 ± 0.20	*	1.07	0.38
ρ SSC (deg)	0.22 ± 0.14	0.32 ± 0.21		0.54	0.63
σ SSC (deg)	0.31 ± 0.21	0.18 ± 0.15		0.68	0.47
nf SSC	0.01 ± 0.01	0.01 ± 0.00		0.02	0.01

s.d. = one standard deviation and n = 10 nonsmoothed and 10 smoothed images, *p < 0.05.

TABLE 2
Errors in Registration of FDG Brain Images Where One Image Was a Simulated Hemispherectomy

	Average error ± s.d.		$p < 0.05$	Maximum error	
	SAD	SSC		SAD	SSC
x (mm)	0.79 ± 0.50	0.72 ± 0.55		2.08	1.80
y (mm)	0.34 ± 0.18	0.44 ± 0.32		0.77	1.17
z (mm)	2.83 ± 1.77	2.66 ± 1.78		7.75	7.55
θ (degrees)	0.42 ± 0.60	0.42 ± 0.60		1.70	2.02
ρ (degrees)	2.42 ± 1.80	2.43 ± 1.78		7.38	7.28
σ (degrees)	1.63 ± 3.00	1.70 ± 2.94		10.1	9.94
nf	0.006 ± 0.004	0.005 ± 0.005		0.01	0.02

s.d. = one standard deviation; n = 10 images.

original pixel grey scale value, such that intense brain activity is assigned the same value as noise or reconstruction artifacts which may also be above the contour threshold. On the other hand, by including the SAD method within the contour, the grey scale intensity of the pixel was used as an additional factor in the similarity measure. The advantage of combining a threshold segmentation and a pixel intensity subtraction in a similarity measure can be illustrated in the situation of registering exact spherical objects. With the Chen-Pellazari method, spheres cannot be rotationally registered; however, if the spheres contain a nonuniform grey scale intensity pattern within their volumes, they can be registered using the SAD or SSC methods.

The SSC method relied on the amount of similar image surfaces. During the calculation of the SSC, image surfaces that are outside the range of the noise fluctuations are treated the same regardless of the magnitude of their pixel value differences. Therefore, a dissimilar image area consisting of extreme grey scale pixel values will result in the same SSC measure as the same sized area which has only a mild difference in pixel values, i.e., where the magnitude of the differences is just above the noise and intensity surface overlaps. Although linear measures of image similarity such as the SAD will try to minimize these extreme differences and possibly result in a misregistration, we did not find this occurring in our results. In addition, the noise in the reconstructed PET images is not truly poisson in distribution, and it may be possible that the addition of the periodic change in grey scale intensities (5% of pixel grey scale value) was not sufficient to overlap the filtered backprojection reconstruction artifacts in the PET images.

Sharp interfaces in one of the images did not affect the performance of the registration since it is the absolute difference in the image sets that contributes to the SAD measure. On the other hand, the SSC method which depends on the number of changes in the subtraction image, will result in a higher SSC measure if there are more sharp interfaces in a given pair of images when compared to images with smooth grey scale intensity interfaces. Although this will increase the SSC in a given pair of images,

at optimum registration there should still exist a maximum SSC measure.

The SAD algorithm that we implemented was computationally fast in that only floating point subtractions and additions were required. The SAD method also had the advantage of being a continuous and differential function so that the simplex method of function optimization could be used, and most registrations converged to a result usually within 10 min using a low-end workstation. More efficient numerical methods of function optimization (18) and a faster computer could be used to improve the speed of registration. The speed of the algorithm was due to the systematic omission of pixels which were zero in the binary image mask. The advantage of the row skipping rather than interpolation of the image data into a smaller matrix was in the ease of program implementation accomplished by simply skipping rows in the image data matrix. Although the row skipping caused a nonuniform sampling of data in the y direction, reasonably accurate registration was achieved. It should be noted that the plane separation of 6.75 mm was an even larger interval in the z direction.

In noisy images, exact registration will still produce a nonzero SAD. Improved registration was achieved by preprocessing of an image with a nine-point smoothing filter.

Potential Registration Applications

The ability to register brain, cardiac and liver PET images demonstrates the general purpose utility of the method we implemented and should allow accurate comparison of previously acquired images of the same patient. No symmetry in the object contour is necessary, as required by other proposed methods (13).

The potential applications of this program include the ability to accurately register all acquired frames of a clinical brain study, where the patient may have moved between the frames. The registration of all frames will preserve a high-count brain image, given that the correct attenuation can be applied to each frame as described by Dahlbom (15).

Another application of this program is the detection and quantification of patient movement between rest and stress image myocardial perfusion images. This may be used for

TABLE 3
Average and Maximum Errors in Registration of Normal Nitrogen-13-Ammonia Rest-to-Stress Cardiac Images

| | Average error ± s.d. | | p < 0.05 | Maximum error | |
	SAD	SSC		SAD	SSC
x (mm)	0.47 ± 0.30	0.35 ± 0.23		0.74	0.77
y (mm)	0.43 ± 0.40	0.42 ± 0.27		1.25	1.01
z (mm)	0.83 ± 0.38	0.75 ± 0.39		1.52	1.13
θ (degrees)	0.70 ± 0.24	0.96 ± 0.34		1.11	1.44
ρ (degrees)	1.52 ± 0.46	1.19 ± 0.55		2.14	1.83
σ (degrees)	1.58 ± 0.57	1.16 ± 0.57		2.58	2.05

s.d. = one standard deviation; n = 10 images.

TABLE 4
Average and Maximum Errors in Registration of Abnormal Nitrogen-13-Ammonia Stress-to-Rest Cardiac Images

| | Average error ± s.d. | | p < 0.05 | Maximum error | |
	SAD	SSC		SAD	SSC
x (mm)	0.71 ± 0.37	0.57 ± 0.34		1.33	1.26
y (mm)	0.51 ± 0.48	0.61 ± 0.55		1.76	2.22
z (mm)	1.10 ± 0.84	1.22 ± 0.88		3.31	3.35
θ (degrees)	0.65 ± 0.32	0.99 ± 0.44		1.49	2.01
ρ (degrees)	1.52 ± 0.88	1.61 ± 0.88		2.99	2.57
σ (degrees)	1.73 ± 1.00	1.03 ± 0.94		4.83	4.07

s.d. = one standard deviation; n = 30 images.

TABLE 5
Average and Maximum Errors in Registration of FDG Liver Images

| | Average error ± s.d. | | p < 0.05 | Maximum error | |
	SAD	SSC		SAD	SSC
x (mm)	0.53 ± 0.16	1.25 ± 0.34	*	0.77	1.88
y (mm)	0.31 ± 0.23	0.57 ± 0.31		0.93	0.74
z (mm)	0.36 ± 0.17	0.36 ± 0.16		0.64	0.59
θ (degrees)	0.09 ± 0.07	0.22 ± 0.13	*	0.21	0.38
ρ (degrees)	0.20 ± 0.31	0.26 ± 0.26		1.07	0.91
σ (degrees)	0.27 ± 0.11	0.36 ± 0.27		0.40	0.79
nf	0.008 ± 0.006	0.018 ± 0.009	*	0.02	0.03

s.d. = one standard deviation; n = 10 images.

TABLE 6
Average and Maximum Errors in Registration of FDG Liver Images with Simulated Defects

| | Average error ± s.d. | | p < 0.05 | Maximum error | |
	SAD	SSC		SAD	SSC
x (mm)	0.86 ± 0.59	0.73 ± 0.66		1.94	1.89
y (mm)	0.82 ± 0.87	1.10 ± 1.02		2.68	3.48
z (mm)	1.25 ± 1.14	1.25 ± 1.13		3.92	3.84
θ (degrees)	0.65 ± 0.57	0.64 ± 0.51		1.53	1.37
ρ (degrees)	0.78 ± 0.89	0.77 ± 0.82		3.00	2.67
σ (degrees)	1.12 ± 1.03	1.43 ± 1.33		2.89	3.95
nf	0.032 ± 0.027	0.024 ± 0.024		0.08	0.07

s.d. = one standard deviation; n = 10 images.

quality control. In addition, the quantified movements can be transformed into the movement parameters required to register the unreconstructed sinogram data to the transmission scan for accurate attenuation correction during image reconstruction (3), assuming that no patient movement occurred between the transmission and first emission scan. Moreover, if patient mispositioning (between transmission and the second emission scanning) can be corrected, then treadmill exercise imaging with PET would be potentially feasible, where the stress emission scan can be registered to the resting emission scan so that the same attenuation correction can be used during reconstruction. Likewise, cardiac viability studies using FDG may have their uptake periods outside the scanner, thus allowing another procedure to be performed on the scanner during this time. Another application of cardiac registration is that the same set of reslice parameters may be used for generating short axis rest and stress images without operator variability.

CONCLUSION

We have implemented and compared both the SAD and SSC methods for three-dimensional automated registration of low count and dissimilar PET images. No significant advantage in the accuracy of registration was found using the SSC method over the SAD method. Both methods gave average errors in registration that were less than 1 ± 1 mm in the translational directions and less than 1 ± 1 degree in the rotational directions.

REFERENCES

1. Phillips RL, London ED, Links JM, Cascella NG. Program for PET image alignment: effects on calculated differences in cerebral metabolic rates for glucose. *J Nucl Med* 1990;31:2052-2057.
2. McCord ME, Bacharach SL, Bonow RO, Dilsizian V, Cuocolo A, Freeman N. Misalignment between PET transmission and emission scans: its effect on myocardial imaging. *J Nucl Med* 1992;33:1209-1214.
3. Harris GC, Hoh CK, Dahlbom M, et al. Development of an automated registration algorithm for detection and correction of patient movement in cardiac PET imaging [Poster]. *Clin Nucl Med* 1992;17:768.
4. Svedlov M, McGuillem CD, Anuta PE. Image registration: similarity measure and preprocessing method of comparison. *IEEE Trans Aerosp Electron Sys* 1978;10:141-149.
5. Barnea DI, Silverman HF. A class of algorithms for fast digital image registration. *IEEE Trans Computers* 1972;21:179-186.
6. Venot A, Lebruchec JF, Roucayrol JC. A new class of similarity measures for robust image registration. *Comput Vis Graph Image Process* 1984;28:176-184.
7. Pelizzari CA, Chen GTY, Spelbring DR, Weichselbaum RR, Chen CT. Accurate three-dimensional registration of CT, PET, and/or MR images of the brain. *J Comput Assist Tomogr* 1989;13:20-26.
8. Woods RP, Cherry SR, Mazziotta JC. Rapid automated algorithm for aligning and reslicing PET images. *J Comput Assist Tomogr* 1992;16:620-633.
9. Venot A, Leclerc V. Automated correction of patient motion and gray values prior to subtraction in digitized angiography. *IEEE Trans Med Imag* 1984;3:179-186.
10. Venot A, Liehn JC, Lebruchec JF, Roucayrol JC. Automated comparison of scintigraphic images. *J Nucl Med* 1986;27:1337-1342.
11. Liehn JC, Amico S, Delisle MJ, Flament JB. Improvement of parathyroid Tl-Tc scintigraphy by using a new image subtraction method. *Eur J Nucl Med* 1988;14:184-189.
12. Bonnet N, Liehn JC. Image registration in electron microscopy: application of a robust method. *J Elect Microsc Techn* 1988;10:27-33.
13. Minoshima S, Berger KL, Lee KS, Mintun MA. An automated method for rotational correction and centering of three-dimensional functional brain images. *J Nucl Med* 1992;33:1579-1585.
14. Venot A, Golmard JL, Lebruchec JF, et al. Digital methods for change detection in medical images. *Proc Internat Conf Inform Process Med Imaging* Nijhof, The Hague 1984;1-16.
15. Siegel S, Dahlbom M. Implementation and evaluation of a calculated attenuation correction for PET. *IEEE Trans Nucl Sci* 1992;39:1117-1121.
16. Pronzato L, Walter E, Venot A, Lebruchec JF. A general purpose global optimizer: implementation and application. *Math Comput Simul* 1984;28:412-422.
17. Nelder J, Mead R. The simplex method for function minimization. *Comput J* 1965;7:308-313.
18. Press WH, Flannery BP, Teukolsky SA, Vetterling WT. *Numerical recipes in C*. New York, NY: Cambridge University Press, 1988;305.